MDPI

Article

Ablation-Dominated Arcs in CO2 atmosphere - Part II: Molecule emission and absorption

Ralf Methling [1,†]*, Nicolas Götte [2,†], and Dirk Uhrlandt [1,†]

[1] Leibniz Institute for Plasma Science and Technology (INP), Felix-Hausdorff-Str. 2, 17489 Greifswald, Germany; methling@inp-greifswald.de

[2] Institute for High Voltage Technology, RWTH Aachen University, Schinkelstrasse 2, 52056 Aachen, Germany; e-mail@e-mail.com

* Correspondence: methling@inp-greifswald.de; Tel.: +49-3834-554-3840

† These authors contributed equally to this work.

Version August 11, 2020 submitted to Energies

Abstract: Molecule radiation can be used as a tool to study colder regions in switching arc plasmas like arc fringes in contact to walls and ranges around current zero (CZ). This is demonstrated in the present study for the first time for the case of ablation-dominated high–current arcs as key elements of self–blast circuit breakers. The arc in a model circuit breaker (MCB) in CO2 with and an arc in a long nozzle under ambient conditions with peak currents between 5 and 10 kA were studied by emission and absorption spectroscopy in the visible spectral range. The nozzle material was polytetrafluoroethylene (PTFE) in both cases. Imaging spectroscopy was carried out either with high-speed cameras or with intensified CCD cameras. A pulsed high-intensity Xe lamp was applied as background radiator for the broad-band absorption spectroscopy. Emission of Swan bands from carbon dimers was observed at the edge of nozzles only or across the whole nozzle radius with highest intensity in the arc center, depending on current and nozzle geometry. Furthermore, absorption of C2 Swan bands and CuF bands were found with the arc plasma serving as background radiator. After CZ, only CuF was detected in absorption experiments.

Keywords: circuit breaker; switching arc; optical emission spectroscopy; optical absorption spectroscopy; current zero; SF6 alternative gases; CO2; PTFE; Swan bands; CuF

1. Introduction

Self-blast circuit breakers represent one of the main technologies for high-current interruption at high voltage. After contact separation, intense radiation emitted from the high–current arc leads to a considerable photo–ablation of the surrounding nozzle which causes a pressure build up and finally a strong gas flow necessary for arc quenching around current zero (CZ) [1,2]. Polytetrafluoroethylene (PTFE) is typically used as the nozzle material and SF_6 as the filling gas. However, the substitution of the greenhouse gas SF_6 by more environment–friendly gases like CO_2 is an actual trend. The pressure build up due to strong arc radiation and nozzle ablation as well as the arc quenching processes are key issues of the successful current breaking and have been subject of a large number of scientific studies. Main questions concern the properties of the arc and the hot gas regions like temperatures and species densities which are required for a sufficient understanding of the processes. Optical methods like emission and absorption spectroscopy can provide such quantities under the demand that arc and hot gas regions are optically accessible. However, an optical access can only be realized by adapted construction of specific model circuit breakers (MCB) or by appropriate model experiments [3–5].

Meanwhile, a sufficiently good knowledge of the arc properties during the high–current phase and in the high temperature regions (above 6 000 K) of the arc has been developed from spectroscopic

studies of switching arc experiments and MCBs (see e.g. [3]). This is because atomic and ionic species dominate in the high temperature regions and generate an intense spectral line radiation which can be well used for the determination of temperatures and species densities [6–8]. However, the analysis of low-temperature regions of the arc fringes, of the regions near nozzle walls and of the temporal phase of arc quenching is much more challenging due to low line radiation intensities.

The investigation of the phase around current zero by optical emission spectroscopy (OES) and the determination of arc temperatures during the arc quenching as close as possible to CZ was a topic of our accompanying paper [9]. An MCB using CO_2 as a filling gas and a PTFE-nozzle experiment under ambient air were used for the analysis of line radiation of oxygen and fluorine atoms as well as of carbon ions. Both setups will be also used in this study and explained shortly in section 2.

It is well known from composition calculations of thermal plasmas that the dissociation of filling gases like SF_6 and CO_2 and reactions with the ablation product C_2F_4 and metal vapor from electrode erosion can produce a number of molecular species in an intermediate temperature range before an almost complete dissociation to atoms occurs at higher temperatures (see e.g. [10]). Hence, the study of molecule radiation can help to analyze the interesting ranges of lower temperatures near the nozzle boundaries and in the arc quenching phases. Unfortunately, there is a very low number of such studies for arcs in corresponding gas mixtures and particularly for switching arcs.

Interesting candidates for the study of molecule radiation are the Swan-bands of the C_2 molecule (around 500 nm) or the violet band of CN (around 385 nm) because of the relatively intense radiation in the optical range. Emission and absorption spectroscopy of the C_2 radiation have been used for example to study the structure of carbon arcs for nanoparticle synthesis [11–13]. The radiation of CN was analyzed in a study of the arc ablation of organic materials in ambient air with close relation to low-voltage switching [14]. Furthermore, both molecules have been more intensely studied in plasmas produced by laser ablation or in the laser–induced breakdown [15–19].

The occurrence of C_2 molecules is expected in switching arcs in CO_2 atmosphere or in the case of ablation of PTFE or organic wall materials. For laser irradiation it was reported that the dominant mechanism for the production of C_2 molecules at low power is the collision of electrons with larger molecules like C_3, C_4 followed by photo–defragmentation whereby one of the emitted products is an exited C_2 molecule. At higher laser irradiance, the Swan band emission is mainly caused by excitation resulting from electron–ion and ion–ion recombination [15]. The shape of continuum is influenced by pressure and temperature. Thus, an estimation of the vibrational temperature can be obtained by comparison of measured and simulated spectra [16,18]. Temperatures in a thermal argon plasma interacting with various insulating plastic materials at magnetically forced arc movement [20] and temperature decay of thermal plasmas caused by polymer ablation using inductively coupled plasma irradiation [21] were investigated experimentally and numerically. As an example of a switching arc study, the absorption spectrum of the C_2 Swan bands was analyzed in a low-voltage circuit breaker model [22]. An arc moving between polyethylene walls was considered, and the density and the rotational temperature of the C_2 molecules were determined from the absorption spectrum which indicates the ablation of the plastic walls. Reports on the analysis of molecule radiation, the C_2 Swan bands in particular, in high-voltage switching experiments as representative for high–voltage circuit breakers are missing so far.

During the OES study of a MCB and a nozzle experiment described in our first paper [9], molecule radiation of C_2 and CuF was recorded under different conditions and to some extent in unexpected ranges of the arc. The molecule CuF is expected when copper vapor from the electrode erosion is mixed with the dissociated PTFE vapor from the nozzle ablation [10]. The results for molecule emission and absorption should be given in this second paper in detail. The aim is to demonstrate the occurrence of molecule radiation as a possible candidate to characterize low–temperature regions in self–blast circuit breakers as well as ablation processes. However, determination of quantities like rotational temperatures and densities is out of the scope of the present paper. The MCB and nozzle experiment

setups will be presented shortly in section 2 together with the setup for spectroscopic measurements because details can be found in [9]. Results are given in section 3 followed by a discussion in section 4.

2. Materials and Methods

Two setups of electrodes and nozzles were used. They are described in detail in an accompanying paper [9]; basic features are sketched in Figure 1. Actually, the majority of experiments described in this paper were carried out with setup (b) and only few with setup (a). The electrodes were made of W–Cu with a 10 mm diameter and had a fixed distance of 40 mm. Nozzles made of PTFE doped with $<$0.5 wt% molybdenum disulfide (MoS_2) with an inner diameter of 12 mm were placed around the electrodes: Either setup (a) was applied with one 126 mm long, tubular shaped nozzle of 50 mm outer diameter for strong ablation and high pressure built-up or setup (b) was used with two nozzles of about 50 mm length and 104 mm outer diameter separated by 4 mm distance to form a heating channel. At the electrode positions, the nozzle diameter was increased to about 16 mm for an exhaust gas flow.

The arcs were operated either under ambient conditions (setup (a)) or in a vessel filled with 1 bar CO_2 (setup (b)) as part of a model circuit breaker similar to [3]. Windows in both the model chamber and the vessel allowed a free view through the nozzle and hence absorption experiments.

Sine–like currents were applied, for setup (a) with about 100 Hz frequency and 11 kA peak current and for setup (b) with 50 Hz and 5.3 kA. Thin Cu wires were used to initiate the arc discharges. Currents were measured using Rogowski coils. In case of setup (b) a pressure sensor (603A from Kistler) was placed in the heating volume of the model circuit breaker.

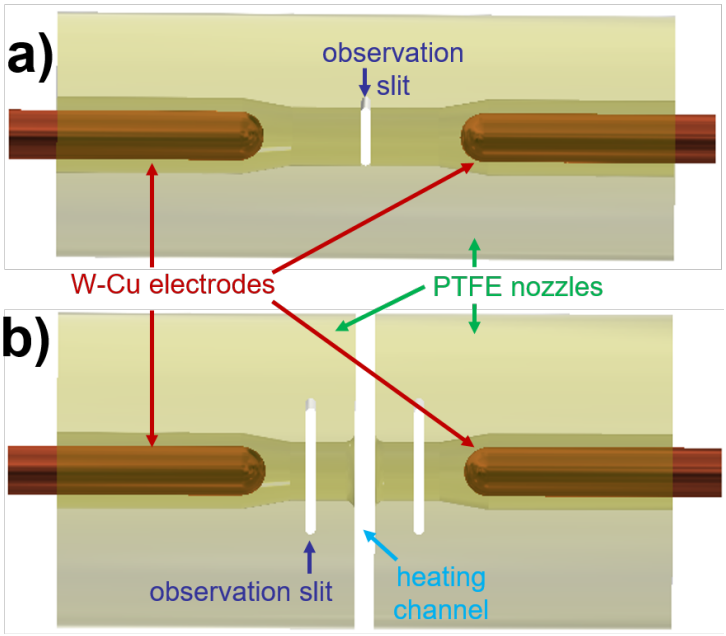

Figure 1. Setups (**a**) with a closed, long PTFE nozzle for experiments with strong ablation and high pressure built-up and vertical observation slits in the middle and (**b**) with two separated PTFE nozzles forming a heating channel for plasma flow into a heating volume as used for the model circuit breaker.

Optical access was realized by vertical slits of 2 mm width that were sealed by 2 mm–thick quartz plates, ranging over the complete nozzle diameter. After each shot the sealing plates were checked visually and exchanged; the transmission was measured regularly. Pairwise placement at opposite positions enabled background illumination and absorption measurements. For setup (a) the observation slits were placed in the middle between both electrodes. In setup (b), the observation point was positioned in one of the nozzles at half distance between electrode tip and nozzle exhaust, i.e. $\sim$9 mm away from both. On the left side of Figure 3, an image of the HSC observation area (grey scale image) including the OES axis (yellow dashed line) is shown.

Different methods were applied for the optical analysis. Firstly, high-speed cameras (HSC) from Integrated Design Tools (IDT) were used to observe the general discharge behavior: Y6 with 24bits color or Y4 with 10bits monochrome. Secondly, optical emission spectroscopy was carried out by means of an imaging spectrograph with 0.5 m focal length (Roper Acton SpectraPro SP2500i). The nozzle slit was imaged on the entrance slit of the spectrograph by a focusing mirror to spectrally investigate arc cross sections, i.e. perpendicular to the arc axis. Using the spectrograph with Y4 HSC enabled to record series of 2D–spectra with typical repetition rates of 100 μs (frame rate 10 kfps), allowing rather long exposure times up to 98 μs that were necessary due to limited camera sensitivity. Alternatively, the HSC could be replaced by an intensified CCD camera (PI-MAX4 from Princeton Instruments) with higher sensitivity, allowing single frame acquisition of shorter exposure times even at lower intensities, e.g. around current zero. In a compromise between light intensity, spectral resolution, and exposure time, the entrance slit of the spectrograph was set to 50 μm. With gratings of 150 lines per mm for overview and 1 800 l/mm for detailed spectra, the spectral range was 150 nm and 10 nm and the spectral resolution 0.3 nm and <0.1 nm, respectively. The intensity of side-on spectra was calibrated in units of spectral radiance by means of a tungsten strip lamp (OSRAM Wi 17/G) at the arc position. The window transmission of 50–70 % was taken into account, mainly resulting from the coating of the quartz plates at the nozzles.

Thirdly, broadband absorption spectroscopy was carried out around CZ. Therefore, a background illumination was required with radiances higher or comparable to the emission of the arc. It was supplied by a pulsed high-intensity xenon lamp with a radiance similar to a Planckian radiator of 12 000 K [23]. The square shaped pulse had about 1 ms–width at about 1 MW electric power, delivering a nearly constant emission intensity during the plateau phase.

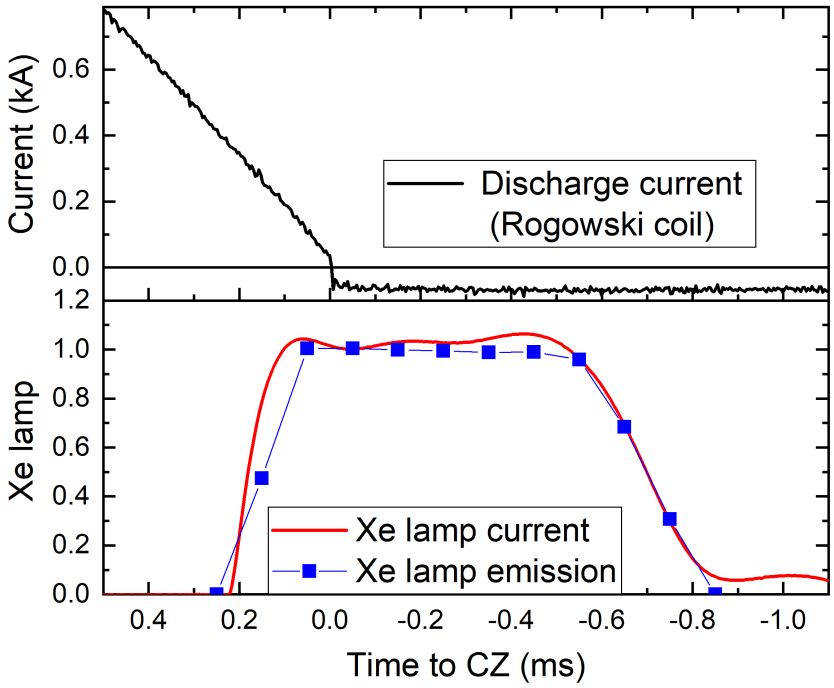

Figure 2. Top: Arc current at the end of discharge. Bottom: Xe lamp current (red) and development of its emission intensity (blue squares).

Figure 2 shows exemplary current waveforms of the arc discharge around current zero (top, offset after CZ is caused by the Rogowski coil) and the quasi-rectangular pulsed current of the xenon lamp (bottom, red) as well as the spectrally integrated intensity measured by video spectroscopy (spectral range 400–800 nm). Since the electric pulse feeding the Xe–lamp was not perfectly rectangular, a heating phase of the xenon lamp could be observed. Thus, several Xe atomic lines were found in the first 100-200 μs of the 1 ms–pulse before transition towards the 12 000 K–continuum emission.

Additionally, with decreasing current also the emission intensity decreased. Hence, for the OAS analysis only the lamp's plateau phase was applied with a duration of about 700 μs. This relatively long, stable phase allowed for temporal investigation of absorption, e.g. compared to Z–pinches with some 10 μs of varying radiation intensity as used in [22].

3. Results

In order to avoid doubling, some more general results that were already described and discussed in the accompanying paper will not be repeated here. That relates to electrical waveforms, temporal evolution of pressure and plasma composition in the nozzle, and video observation by HSC with and without filtering. Additionally, only selected moments from the overview video spectroscopy will be shown that are mandatory for the discussion of molecule emission and absorption. It should be noted that for easier comparison all points in time are given with respect to the current zero crossing.

First, experiments in the MCB (setup (b)) with the sine-like current up to 5.3 kA are considered. The arc voltage was around 200 V (after peak caused by explosion of ignition wire) until the arc extinction peak some hundred μs before CZ. The total pressure in the nozzle started from filling pressure of 1.0 bar to a maximum of 3.5 bar close to peak current and decreased to about 2.0 bar at current zero. After ignition, an arc discharge in CO_2 atmosphere was observed, also containing copper from ignition wire and electrodes. Within the next few hundreds of microseconds, the ablation of the PTFE (C_2F_4) wall material started to dominate the discharge, blowing the CO_2 out of the nozzle. In the following, a long and stable period was observed that was dominated by ablation. Another reversal of flow was found about 2 ms before CZ: With decreasing arc current, the wall ablation and thus the pressure in the nozzle decreased to values below that in the heating volume. Hence, relatively cold gas from the heating volume with high fraction of CO_2 flowed back into the nozzle. In the last ms, only emission from O I was observed, indicating a plasma composition completely dominated by CO_2.

3.1. Analysis of C2 Swan bands

An example of a two-dimensional spectrum is shown in Figure 3. It was acquired with setup (b) shortly before peak current (7.3 ms to CZ). The vertical axis represents the position along the observation slit in the nozzle, cf. dashed yellow line in the HSC image on the left side; the horizontal dimension is given by the wavelength in the spectral range ∼480-625 nm. The arc discharge was dominated by wall–ablation at that point in time; no emission from copper or oxygen but lines from atomic fluorine F I and atomic and ionic carbon lines C I, C II could be observed. This radiation was mainly emitted in a broad distribution over the arc cross section with highest intensities in central positions, as it is typical for wall–stabilized arcs with broad and flat temperature profile [9]. However, an additional structure can be recognized with a different lateral distribution: A dense pattern of lines with increasing intensities and numbers towards higher wavelengths with abrupt breaks at positions near 516 and 564 nm, spread over the whole nozzle diameter and partly even with maxima close to the wall. This structure has been attributed to the Swan band system originating from transitions between the $d^3\,\Pi_g$ and the $a^3\,\Pi_u$ electronic states of C_2 molecules. Four cases of appearance of Swan bands in the discharge will be presented in the following.

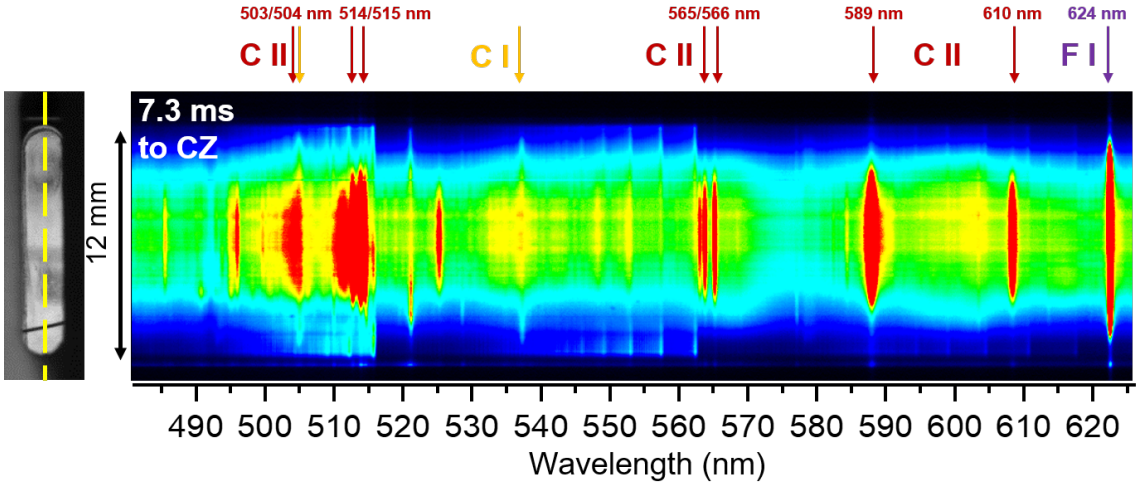

Figure 3. Left: Photo (grey) of observation window. Right: Two-dimensional optical emission spectroscopy frame at 7.3 ms before CZ.

Firstly, the Swan bands occurred at the outer edges of the arc preferably close to the nozzle walls as shown in Figure 3. Generally, this can be regarded as typical behavior for cases of moderate PTFE influence, i.e. when current density is not too high and the temperature close to the wall is rather low, allowing existence of carbon dimers.

Secondly, other Swan band pattern were observed over the full vertical axis of the side–on 2D–spectra. The example shown in Figure 4 was acquired with setup (b) about 6 ms before CZ, i.e. shortly before the peak current. A grating of 1800 l/mm was applied to obtain higher spectral resolution. A good agreement was found of the 1D-spectrum taken in central position with spectra shown by Camacho in OES studies of a plume produced by laser ablation of a graphite target [17]. The weaker continuum and stronger C II lines compared to [17] hint on rather high plasma temperatures at least in the arc center with higher current density than near to the wall.

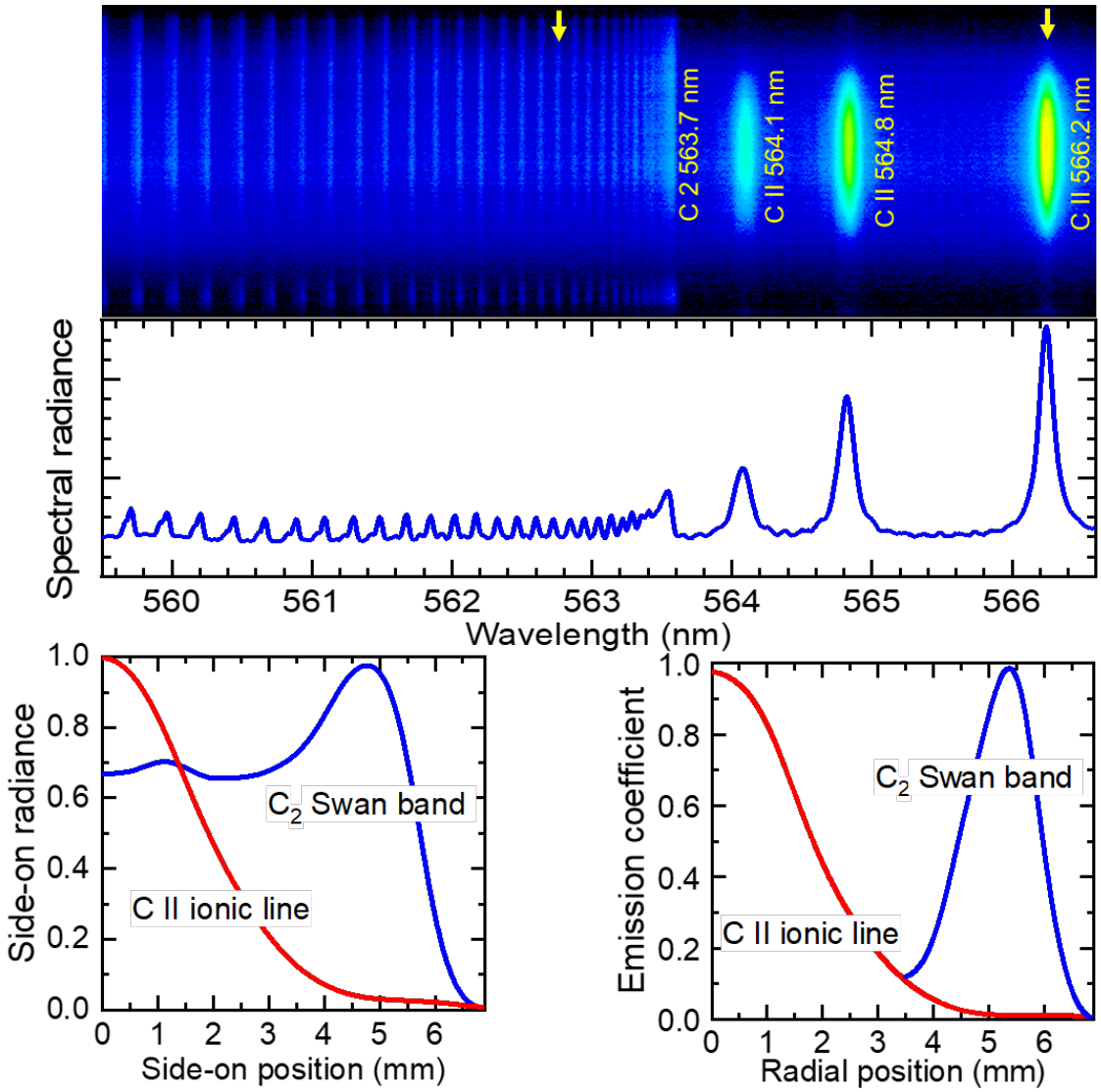

Figure 4. Top: 2D spectrum over the full arc cross section (upper part) together with the corresponding 1D–spectrum from central arc position (lower part) in the spectral range around the C_2 Swan band head at 563.7 nm - Swan band on the left side and C II lines on the right side. Bottom left: Spectrally integrated line intensities of the carbon ion line C II 566.2 nm and of the C_2 Swan band line at 562.8 nm, labeled by yellow arrows. Bottom right: Inverse Abel transformation carried out for these intensities to reveal origin of emission.

Exemplarily, one of the lines of the C_2 Swan band near 562.8 nm was analyzed; the carbon ionic line at 566.2 nm was used for comparison, cf. yellow arrows in the 2D–spectrum. The side–on radiances are shown in the lower left part of Figure 4: whereas the ionic line has its maximum in the center, the Swan band emission is spread more homogeneously over wide side–on positions between center and 4 mm but has a distinct maximum near to 5 mm, i.e. near to the wall. Since both emissions showed good symmetry in relation to the center, this axis was used for symmetrization and as central side–on position "0 mm". Then, the radial profile of the emission in the arc can be analyzed by Abel inversion of the side–on radiances. Results are shown in the lower right part of Figure 4. The C II 566.2 nm ionic line is emitted as expected mainly in the center; the emission coefficient decreases to 20% within radial positions of 2 mm. The C_2 Swan band, however, has a sharp peak of less than 2 mm FWHM with a maximum emission coefficient below 1 mm to the wall. It should be noted that although the nozzle diameter is 12 mm some intensity was detected at side–on position above 6 mm due to experimental limitations like quartz plate connection and refraction at the windows. The algorithm of inverse Abel

transformation is limited in case of very low emission from the central position, therefore the C_2 emission coefficient in the center is not plotted for values below 10% (radial positions <3.5 mm). To summarize even in the case of Figure 4 the Swan bands are emitted only in a thin sheath at the wall.

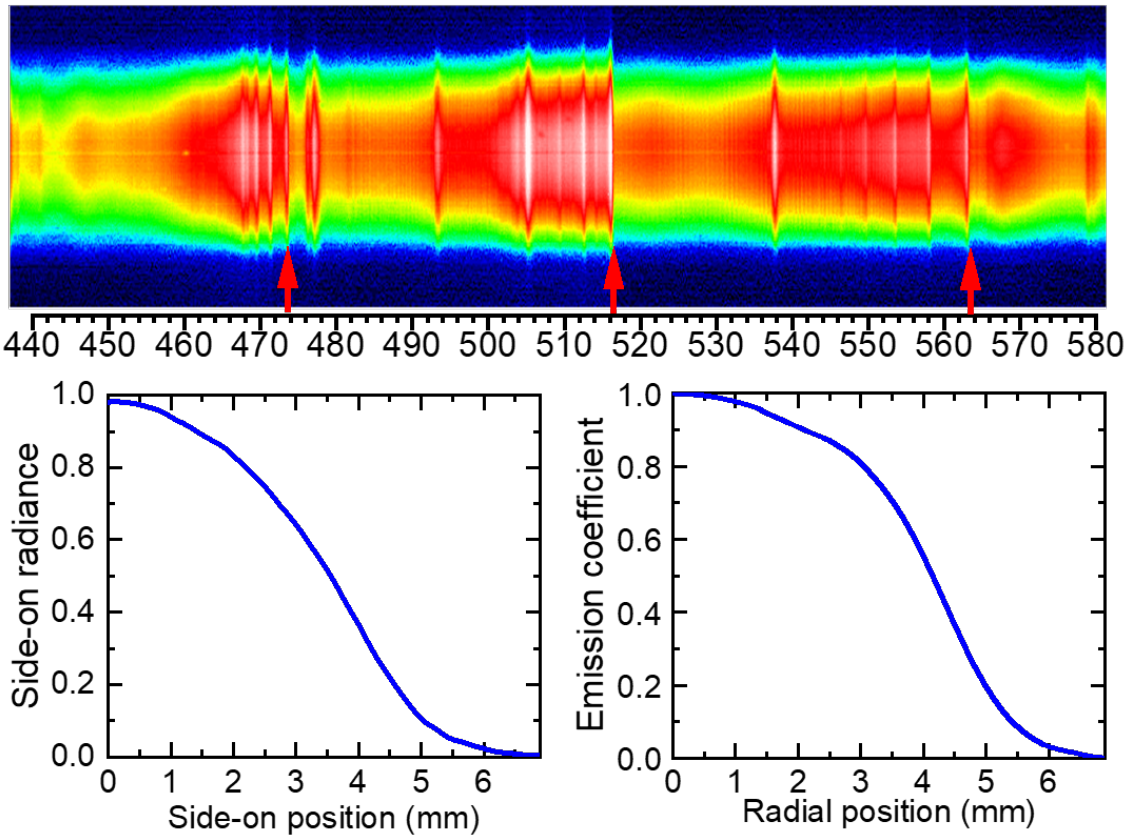

Figure 5. Top: Spectrum acquired 300μs before CZ with setup (a) and 8 kA peak current. It is completely dominated by molecular radiation of C_2 Swan bands (band heads labeled by arrows). Bottom: Spectrally integrated line intensities (left) and emission coefficient obtained from Abel inversion (right) of the C_2 Swan band emission at 562 nm.

A third example for the occurrence of C_2 Swan bands is shown in Figure 5. It was only observed with setup (a) providing higher pressure and strong wall ablation due to peak currents of 8 kA (100 Hz). With the single long PTFE nozzle the current was not switched off and multiple current zero transition were observed. Except the ignition phase and few hundred μs around CZ, all spectra are dominated by pronounced emission of the Swan bands. Its band heads at 473.7 nm, 516.5 nm, and 563.6 nm are indicated by red arrows in the two–dimensional spectrum in the upper part of Figure 5. The wavelength range chosen here does not include the band head at 438.2 nm but also contains the C II lines at 564.06 nm, 564.81 nm, and 566.26 nm as well as the C I atomic lines at 476.2 nm, 477.0 nm, 493.2 nm, 505.2 nm, and 538.0 nm. Weak or non–visible ionic and atomic carbon lines in comparison with the Swan bands give first hint to rather low temperatures in the center of the arc. Furthermore, it was observed that the occurrence of carbon lines drastically changes approaching current zero. Within some 100 μs, first the ionic and than the atomic lines disappear; after CZ they reappear in reversed order. In fact, disappearance of the atomic lines cannot be observed for first and second, but for the third CZ crossing.

The Swan band pattern has much higher intensity in central position though the emission is extended to the side–on positions of the nozzle wall. The origin of emission is further analyzed using the band head around 563 nm as shown in the lower part of Figure 5. The side-on profile (left) and the emission coefficient obtained by inverse Abel transformation (right) reveal a different occurrence in

comparison to the plasma in Figure 4. The Swan bands are emitted with highest intensities in the center of the arc, continuously decreasing towards the nozzle walls. Thus, it can be followed that the arc plasma is completely dominated by PTFE material and it is characterized by rather low temperatures even in the arc center. It should be mentioned that this third case of Swan band appearance is the most extreme and could not be achieved with setup (b) with two nozzles separated by the heating channel even when the peak current was doubled to 10 kA.

The forth example was typical for setup (b): Swan bands appeared as an absorption pattern at currents >4 kA. An example is shown in Figure 6. The spectrum was taken shortly after the current maximum (4.7 kA, 4.6 ms before CZ). Emission from the hot plasma in the arc center served as an internal background radiator that was absorbed by the much cooler carbon dimers near to the nozzle wall. As in Figure 5, the band heads at 473.7 nm, 516.5 nm, and 563.6 nm are indicated by arrows. Additionally to the absorption pattern, some emission lines can be found. These are all C II lines from carbon ions, e.g. at 564.06 nm, 564.81 nm, and 566.26 nm, and are mainly emitted in the center of the arc with higher temperatures. For the above described arcs with strong flow of ablated material towards the electrodes (third and fourth case), no copper lines were visible. The F I lines were not in the chosen wavelength range.

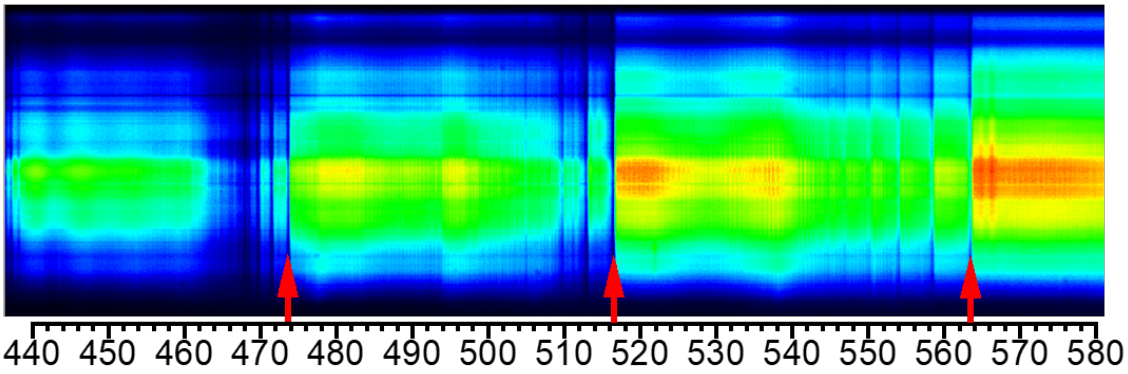

Figure 6. Spectrum during high-current phase of the discharge dominated by molecular radiation of C_2 Swan bands. With setup (b) the Swan bands could be observed as absorption pattern with the plasma in the arc center serving as background radiator. The band heads are labeled by arrows.

3.2. Optical Absorption Spectroscopy around Current Zero

The phase of current zero crossing is of highest importance for an understanding of the switch–off process and the dielectric recovery of the electrode gap region. Hence it is of special interest to extend experimental knowledge as close as possible to CZ and even beyond. However, even tapping the full potential of optical emission spectroscopy, e.g. by application of OES with intensified cameras as described above, the analysis based on optical emission spectroscopy is limited to times about 10 μs before CZ due to reduced energy input by the arc[9]. Consequently, absorption techniques were required for further investigation of the current zero crossing and the immediately following time period. Since the majority of atoms is in the ground state in case of the lower temperatures near CZ, it will be necessary to analyze mainly lines going to ground or very low levels by optical absorption spectroscopy (OAS). However, most of the relevant lines are in deep UV regions far below 300 nm. From the experimental point it is extremely demanding to investigate such radiation under switching–relevant conditions since all components of the setup including high-pressure vessel and model circuit chamber have to be transparent for these wavelengths. With the actual setup even resonant lines that might be more suitable could not be detected due to limited spectral sensitivity of the cameras such as C I at 296 nm or Cu I at 324 nm and 327 nm. The few resonant lines in the available wavelength range above 340 nm have very low transition probabilities, e.g. C I at 462 nm and O I at 630 nm. However, it might be possible that some lines might be occupied around CZ and could be detected by OAS that are characterized by relatively low energy levels and medium transition

probabilities, e.g. Cu I at 510 nm, 570 nm, and 578 nm with E_u=1.39 eV and 1.64 eV or O I at 557 nm with E_u=1.26 eV. Additionally, molecules are possible candidates for absorption, e.g. the C_2 molecule since its Swan bands were observed in emission until few 100 μs before CZ and even in absorption during the high–current phase as shown above.

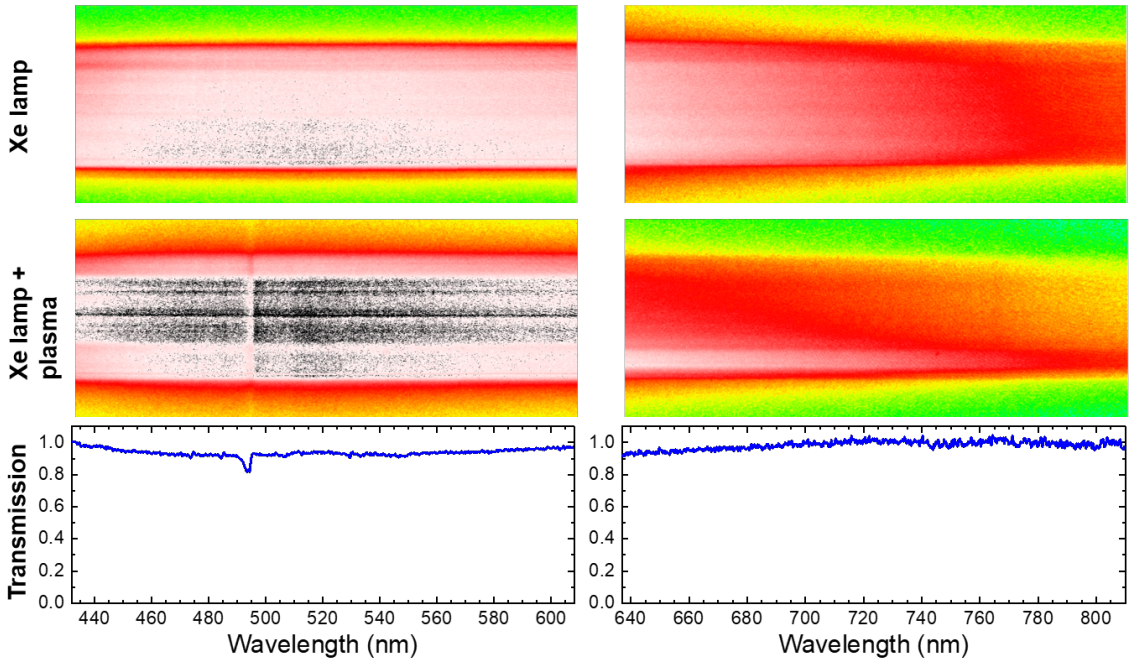

Figure 7. Optical absorption spectroscopy. Top: Overview emission spectra of Xe lamp only. Middle: Xe lamp with discharge of 5 kA peak current and setup (b), acquired at CZ with 50 μs exposure time. Bottom: Spatially integrated transmission calculated from above spectra showing absorption around 500 nm.

Broadband optical absorption spectroscopy (OAS) was carried out around CZ using the pulsed high-intensity xenon lamp as an external wide–band background illumination. Two examples are shown in Figure 7, comprising the wavelength ranges about 440–600 nm (left) and 640–800 nm (right column). In the upper panel only the emission from the Xe lamp is given, i.e. through model circuit breaker including all windows but without discharge. Broadband continuum can be seen in both spectral ranges. It should be noted that the spectra are not calibrated concerning absolute intensity. The edges of the nozzle are indicated by sharp transitions from the bright stripe caused by illumination with the xenon lamp and the dark areas. The spatial distribution within the nozzle slit is quite homogeneous, showing smooth illumination by the background source. In the middle panel, the OES spectra were taken at CZ (exposure time 50 μs) with the Xe lamp continuum passing the remainder of arc discharge in the nozzle. Patterns of horizontal stripes were sometimes observed. Similar experiments using HSC instead of ICCD camera revealed that these stripes did not change from one video frame to the next. Thus, it was reasonable to assume a deposition on the quartz glass sealing the slits, e.g. by particles. In the left spectrum a certain structure was found below 500 nm whereas the right spectrum did not shown any peculiarities. From spectra in top and middle panel a transmission could be calculated, cf. lower panel of Figure 7. For an improvement of the signal–to–noise ratio and a better visualization of the intensity ratio, spatial integration was carried out for determination of the transmission. It revealed that there was only one significant absorption peak around 493 nm. This absorption was clearly accorded to the CuF molecule as will be discussed below. Beside this CuF peak, no hint on any absorbing lines or other features could be detected around current zero, even with the intensified camera with high sensitivity and dynamic range. Even the C_2 Swan bands could not be observed before or after CZ in OAS with the Xe lamp as background radiator although they were detectable in

OES up to few hundred μs before CZ. Moreover, a closer look onto the emission spectra (cf. Figure 3) showed that the CuF absorption at 493 nm could also be found during the high–current phase of the discharge though this effect was rather weak compared to the intense line emission. This will be further investigated in Section 3.3.

Other species for an absorption with maximum around 493 nm could be excluded in detailed spectral analysis, including all relevant elements as Cu and W from electrodes, C, O, and F from filling gas and nozzle, and even H as possible contamination. As an example, a prominent candidate might have been the carbon atomic line C I at 493.20 nm, although its lower energy level of 7.7 eV is rather high. However, this line was not detected in emission like other atomic carbon lines with similar upper level of about 10 eV and comparable transition probabilities in the range of several 10^6 s^{-1}, e.g. C I 505.21 nm and 538.03 nm (cf. Figure 3). Moreover, these C I lines were still observed in emission 0.7 ms before CZ, while at 493 nm an absorption could be seen even during discharge.

Since no absorption spectra were found in literature for CuF, a comparison was carried out with emission spectra of photofragments in a gas phase photochemical fragmentation process excited by 308 nm-laser radiation [24]. In Figure 8, the emission spectrum from Cheon et al. [24] was added as an overlay (black) to the calculated absorption spectrum (dashed blue curve) for comparison. Taking into account the different experimental conditions and methods, a compelling agreement was found. Basic data of the CuF emission are listed in Table 1.

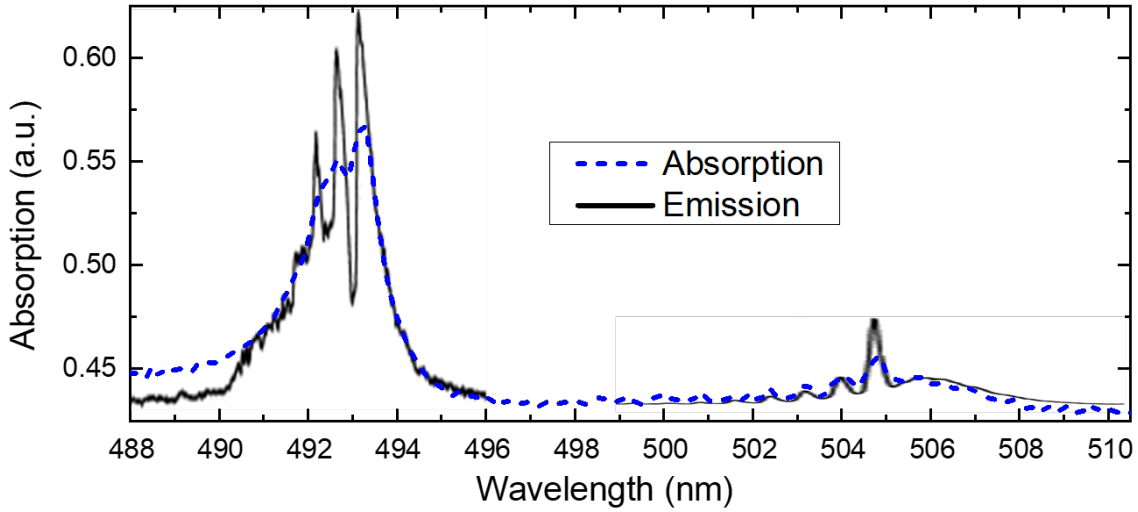

Figure 8. Absorption spectrum around current zero (dashed blue) and comparison with emission spectra of CuF molecules from [24] (black line).

Table 1. Basic data of CuF emission lines [25,26].

Wavelength nm	Relative intensity	Lower level eV	Upper level eV	Transition		Quantum upper	number lower	System
478.19	400	0	2.51	$X^1\Sigma^+$	$C^1\Pi$	0	1	C
490.13	500	0	2.44	$X^1\Sigma^+$	$B^1\Sigma$	0	1	B
492.68	600	0	2.51	$X^1\Sigma^+$	$C^1\Pi$	1	1	C
493.20	800	0	2.51	$X^1\Sigma^+$	$C^1\Pi$	0	0	C
505.23	600	0	2.44	$X^1\Sigma^+$	$B^1\Sigma$	1	1	B
506.11	700	0	2.44	$X^1\Sigma^+$	$B^1\Sigma$	0	0	B
508.64	200	0	2.51	$X^1\Sigma^+$	$C^1\Pi$	1	0	C
567.72	500	0	2.18	$X^1\Sigma^+$	$A^1\Pi$	2	2	A
568.57	600	0	2.18	$X^1\Sigma^+$	$A^1\Pi$	1	1	A
569.43	600	0	2.18	$X^1\Sigma^+$	$A^1\Pi$	0	0	A

In the following, the CuF molecular absorption after current zero should be analyzed in more detail. A series of time–resolved spectra is shown in the upper part of Figure 9. The transmission was calculated based on division of the measured spectra (plasma plus xenon lamp) by a xenon lamp spectrum without discharge. Higher spectral resolution was obtained by the grating with 1800 l/mm. Thus, also the peak structure including maxima at 493.2 nm, 492.7 nm, and 493,2 nm can be clearly recognized in agreement with the emission spectrum of CuF molecules from [24] shown in Figure 8. The overlaying periodic structure is not caused by the plasma in the nozzle since the same structure was also observed for the xenon lamp itself. Probably it was caused by an interference effect of glass plates in the detector. The background intensity increases although the xenon lamp is in its plateau phase.

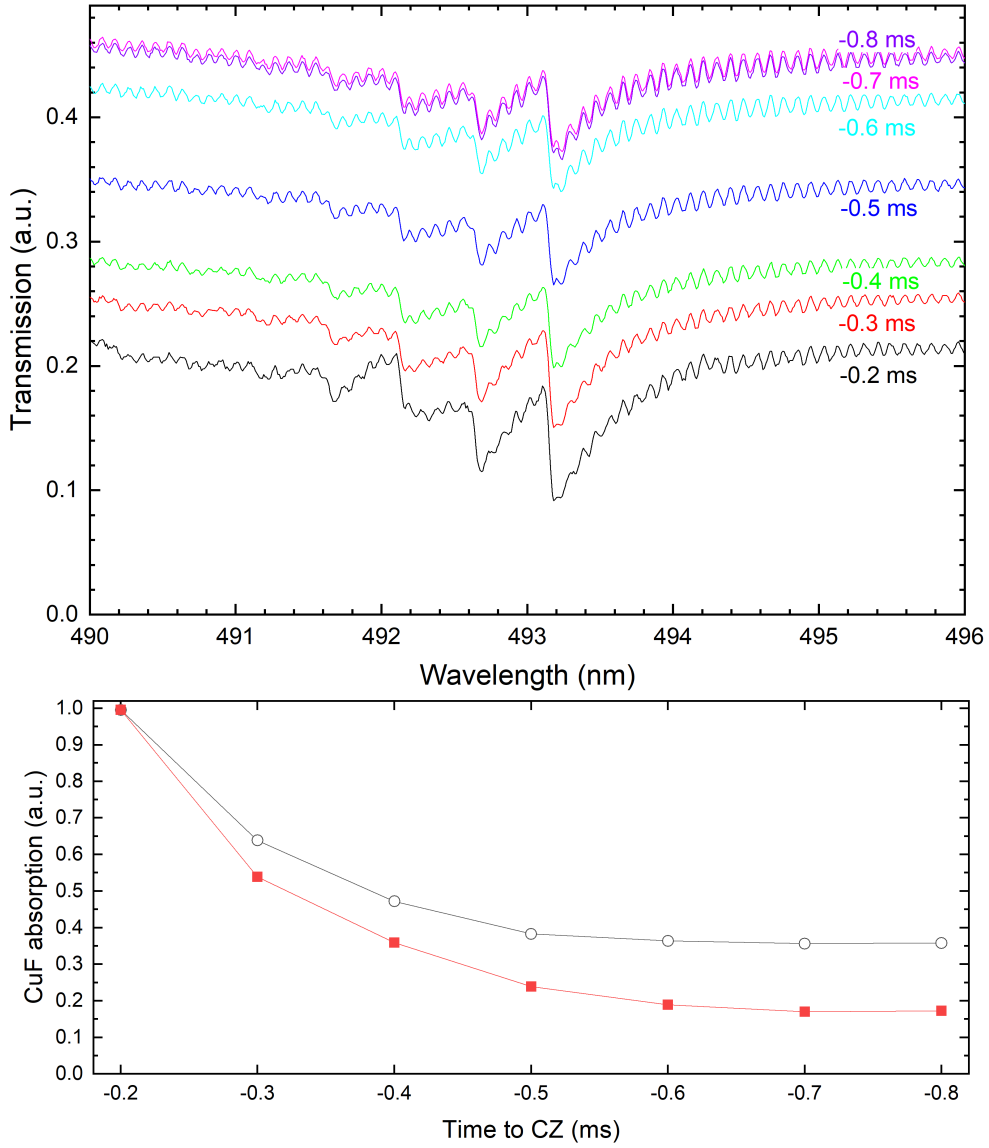

Figure 9. Top: Series of detail transmission spectra after current zero. Bottom: Temporal development of absorption peak at 493 nm calculated as area under curve (AUC, open circles) and AUC normalized by background intensity (filled squares).

For a quantization of the temporal evolution of the absorption, the area under curve (AUC) was determined from the difference between the "background" (average of levels extracted at wavelengths aside the CuF absorption, i.e. around 490 nm and 496 nm) and the transmission, integrated over the spectral range. The AUC is plotted as the curve with black open circles in the lower part of Figure 9.

Additionally, a normalization of the AUC was carried out by division by the (temporally increasing) intensity of the background signal. The normalized AUC is represented by the curve with red filled squares. The spectrum 0.2 ms after CZ was chosen as starting point and the according value was set to 1 for better comparison. Within half a millisecond, the AUC decreases by 60%. The decrease of the normalized AUC is even more significant, namely down to 20% (factor of 5). Few other shots that were carried out confirmed this result. However, due to the exponential nature of this decrease the absolute values are sensitive to the starting point. Summarizing it can be stated that the CuF absorption and thus, also the CuF density decreases after current zero on a timescale of several hundreds of microseconds.

3.3. CuF during high–current phase

As mentioned above, overview OES spectra in Figure 3 gave hint on a possible absorption of the CuF molecule even during the arc discharge though the effect might be considerable lower in absolute intensity than the atomic line emission. Thus, the spectral range around the 493 nm–peak was investigated with video OES of higher resolution (grating 1800 l/mm instead of 150 l/mm, exposure time 98 μs). An example is shown in Figure 10 acquired with setup (b) and 5.3 kA peak current.

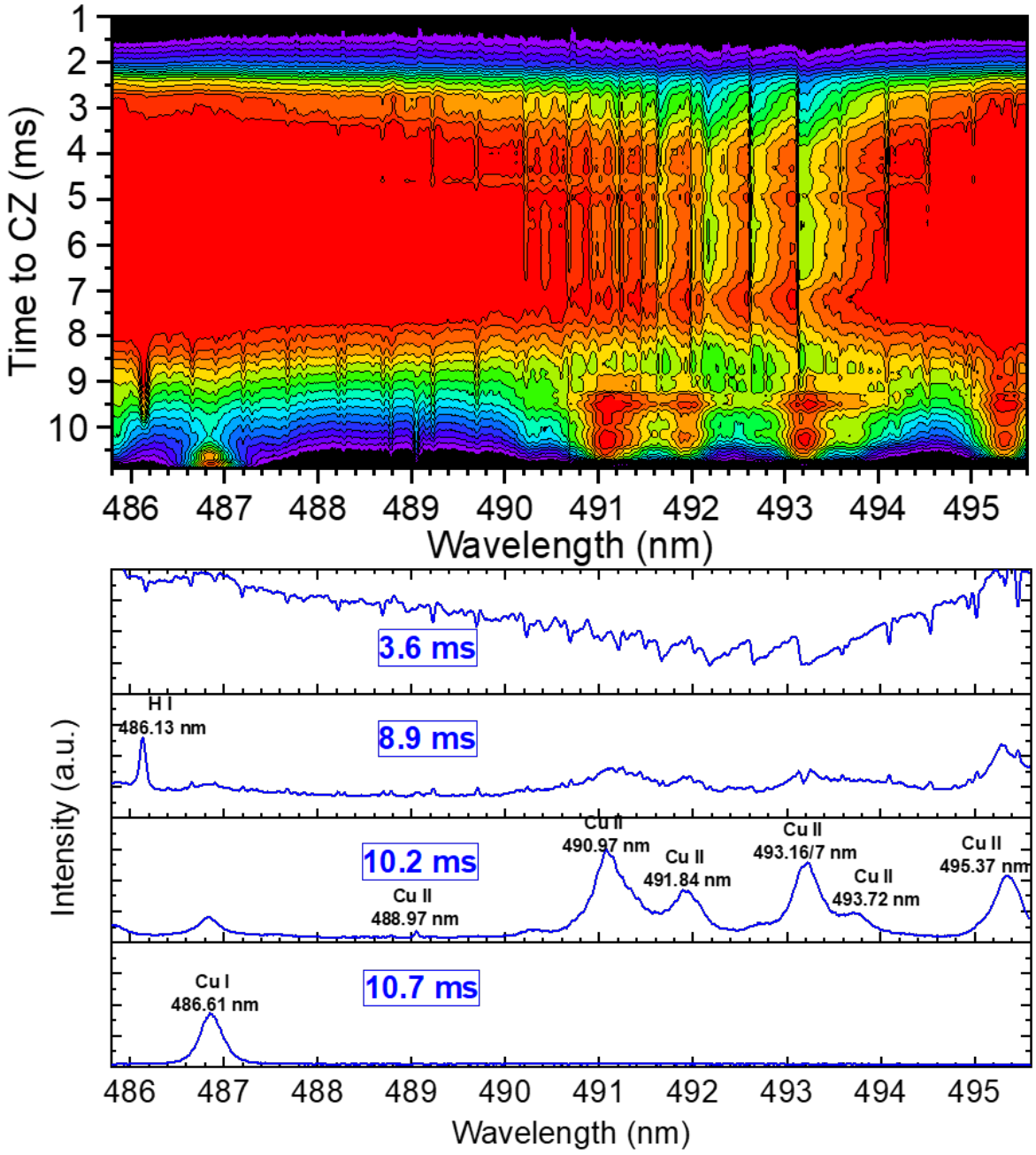

Figure 10. Temporal evolution of the spectral range around 493 nm with CuF absorption (Time to CZ is from bottom to top, the color scale reaches from black for lowest emission to blue, green, and red for highest intensities).

In the upper part, all about 110 optical emission spectra (spatially integrated) are plotted line by line vs. time to CZ, forming a two–dimensional contour plot. In the lower part of Figure 10 a selection of four instants of time with characteristic spectral features are shown. Additionally, several atomic and ionic lines were labeled that helped for fine adjustment and control of exact wavelength positions. The ignition phase the spectra were dominated by atomic and ionic copper line emission. At first, i.e. 10.7 ms before current zero, an atomic copper line Cu I 486.61 nm was observed which was followed by several ionic copper lines. As known from overview OES spectra, the ablation of PTFE was usually initialized about 1 ms after ignition. In the spectral range of Figure 10 no atomic fluorine lines can be observed. However, occurrence of the hydrogen line H_β at 486.13 nm (starting about 9 ms before CZ) can be regarded as an early sign of nozzle ablation, probably caused by a thin remaining

water film on the nozzle surface. Within several hundred microseconds the spectrum is changed from being dominated by copper lines (more probable originating from the W–Cu electrodes than from the ignition wire) to being ablation–dominated. CuF absorption pattern is observed during the full high–current phase, at least from about 8 to 2 ms before CZ. In the spectral range below 500 nm this is basically visible by a broad continuum, starting about 2-3 ms after ignition (or 8 ms before CZ) and lasting at least until about 2 ms before CZ. As can be clearly seen from the top spectrum in Figure 10 the characteristic absorption pattern of CuF can be observed for these 5-6 ms, i.e. during the whole high–current phase of the discharge. Comparable to the case of absorption of the C_2 Swan bands, the CuF absorption is enabled by background continuum from the arc plasma. Observed temporal fluctuation of the intensity has been found to be caused mainly by changes of background intensity, e.g. fluctuation of transmission or reflection due to droplets. Hence, even during the high–current phase a considerable amount of absorbing CuF molecules must be existent in the plasma at nozzle position, i.e. 8 mm away from the electrode. This might be unexpected but leads to the conclusion that the gas flow into the heating channel is strong enough to pull electrode material into the region of optical investigation.

4. Discussion

An ablation-dominated arc of 5 kA peak current was operated in a model circuit breaker with CO_2 atmosphere. Application of a slit over the full radius of the PTFE nozzle enabled direct investigation inside the nozzle. Sealing by thin quartz plates was proved to be an useful method to obtain reproducible conditions of discharges without significant changes of material flow or plasma conditions. Consequent exchange of the plates after each shot yielded to high window transmission with moderate blackening. Only very few cases of reduced sealing quality occurred, easily noticeable after discharges due to increased blackening at the plate's corners. These shots could be repeated with better sealing.

Information was obtained from spatially and temporally resolved video spectroscopy using HSC. That comprised the different phases of discharge and the occurrence of Swan band emission from C_2 molecules. These Swan bands could be observed under varying conditions. Different amount of ablated PTFE from the nozzle wall and plasma temperature were generated depending on nozzle geometry and current density. Firstly, there was an occurrence very close to the nozzle walls as typical behavior for cases of moderate PTFE influence, i.e. when current density was not too high and the temperature close to the wall was rather low, allowing existence of carbon dimers. Although it might be often neglected when the temperature distribution in the arc is investigated, the Swan bands represents the existence of carbon molecules due to wall ablation and thus, an important effect of cooling and change of plasma composition. Secondly, with higher current densities, Swan band pattern were also distributed over the full vertical axis of the side–on 2D–spectra. However, it was found by Abel inversion that the Swan bands are emitted in a thin sheath at the nozzle wall. Thirdly, a different distribution was found under extreme conditions, i.e. with single long PTFE nozzle and high peak currents. The arc plasma was completely dominated by PTFE material and temperatures were moderate in the arc center, proved by weak or non–visible ionic and atomic carbon line emission. The Swan band pattern was emitted with highest intensity in central position though emission was extended to radial positions of the nozzle wall. Finally, Swan bands also appeared as an absorption pattern at moderate currents with setup (b). Emission from hot plasma in the arc center (proved by C II line emission) served as an internal background radiator that was absorbed by the much cooler carbon dimers near to the nozzle wall.

A considerable amount of CuF molecules in the high–current arc as well as near CZ was found from absorption spectra. This was not expected before for several reasons, especially regarding that no other molecules were observed around CZ. A possible explanation is as follows: Around CZ it is expected that convective fluxes are significantly reduced due to equalization of pressures. This allows diffusive expansion of copper from the hot electrode along the nozzle towards the slit position. At the same time there is still some release of fluorine from the PTFE nozzle wall. The chemical reaction

of the fluorine and copper atoms forming CuF molecules could happen at the hot electrode surface followed by evaporation of molecules or in the gas phase with copper atoms evaporated from the electrode. Similarly, the observed absorption during high–current phase might be explained by the gas flow out of the nozzle into the heating chamber. In this case, copper atoms eroded or evaporated from the W–Cu electrode might be flushed with the stream towards the heating channel, reacting on its way with fluorine from the wall, and being detected at the observation slit by absorption with the arc plasma as background radiator. However, during the time immediately after flow reversal, i.e. about 1 ms before CZ, the situation is very different: the gas flow is directed from the heating channel towards the electrodes. Thus, no copper from the electrodes should reach the observation area with the slit and react with fluorine. That means that probably no CuF should be produced at this period; any detected CuF should be survivor from the heating chamber. As a pity, at the moment database is not sufficient to answer the question if there is a lower CuF concentration after flow reversal or not. In the video spectra there is simply not enough background emission to enable sufficient signal for an absorption.

Within the described experiments, limitations of reproducibility, fluctuation in transmission due to particles, film layers on windows, and dust did not allow temporally and spatially resolved determination of the absorption by CuF, e.g. using two–dimensional inverse Abel transformation of video spectra with higher spectral resolution. Nevertheless, this would be the next step if significant technical improvements were done. On the one hand, further optimization of the nozzle slit, its position and manufacturing technique might provide even less changes of the gas and droplet flow conditions, thus allowing measurements still closer to the undisturbed conditions at the nozzle. On the other hand, the observation technique itself might be improved, too. Nowadays, the advantages of intensified and high–speed video cameras can be combined in new generations of cameras or boosters. The background illumination could be improved, too. Beside improvements in the optical path in order to enhance the intensity and homogeneity, the pulsed xenon lamp might also be replaced by a laser–driven light source with extended pulse duration. As a consequence, quantification of the CuF absorption after CZ as well as during the arc discharge might be possible. Furthermore, OAS regarding Swan bands could be tackled. Last not least, tests with other electrodes should be carried out to finally proof the origin of absorption by CuF–molecules, e.g. made of pure tungsten.

Altogether, the possibilities of a recording of molecule radiation emission and absorption in the visible spectral range have been demonstrated for the case of high–current ablation dominated arcs. Using PTFE nozzles, tungsten–copper electrodes and an operation in air or CO_2, the Swan bands of the carbon dimer C_2 and absorption of the CuF molecule were the only detectable radiation patterns. However, these patterns open up ways for a study of interesting ranges in high-current breaking processes like the colder plasma ranges near the nozzle walls and the time around CZ.

Author Contributions: Conceptualization, R.M. and D.U.; methodology, validation, and formal analysis, R.M.; investigation with setup (a), R.M.; investigation with setup (b), R.M. and N.G.; writing–original draft preparation, R.M. and D.U.; project administration, D.U. All authors have read and agreed to the published version of the manuscript.

Funding: This research was funded by Deutsche Forschungsgemeinschaft grant numbers UH 106/13-1 and SCHN 728/16-1.

Acknowledgments: The authors would like to thank Steffen Franke and Alireza Khakpour for experimental help and fruitful discussions. The calculation of plasma composition was realised by Sergey Gortschakow (all Leibniz Institute for Plasma Science and Technology).

Conflicts of Interest: The authors declare no conflict of interest. The funders had no role in the design of the study; in the collection, analyses, or interpretation of data; in the writing of the manuscript, or in the decision to publish the results.

Abbreviations

The following abbreviations are used in this manuscript:

AUC	area under curve
CO_2	carbon dioxide
CuF	copper fluoride
CZ	current zero
ICCD	intensified charge coupled device
HSC	high–speed camera
MoS_2	molybdenum disulfide
OAS	optical absorption spectroscopy
OES	optical emission spectroscopy
PTFE	polytetrafluoroethylene
SF_6	sulfur hexa–fluoride
W–Cu	tungsten–copper

References

1. Ruchti, C.B.; Niemeyer, L. Ablation controlled arcs. *IEEE Trans. Plasma Sci.* **1986**, *14*, 423–434.
2. Seeger, M.; Tepper, J.; Christen, T.; Abrahamson, J. Experimental study on PTFE ablation in high voltage circuit-breakers. *J. Phys. D: Appl. Phys.* **2006**, *39*, 5016–5024.
3. Eichhoff, D.; Kurz, A.; Kozakov, R.; Gött, G.; Uhrlandt, D.; Schnettler, A. Study of an ablation–dominated arc in a model circuit chamber. *J. Phys. D: Appl. Phys.* **2012**, *45*, 305204.
4. Franke, S.; Methling, R.; Uhrlandt, D.; Gorchakov, S.; Reichert, F.; Petchanka, A. Arc temperatures in a circuit breaker experiment from iterative analysis of emission spectra. *J. Phys. D: Appl. Phys.* **2020**, *53*, 385204.
5. Bort, L.; Schultz, T.; Franck, C.F. Determining the time constant of arcs at arbitrary current levels. *Plasma Phys. Technol.* **2019**, *5*, 175–179.
6. Tanaka, Y.; Yokomizu, Y.; Matsumura, T.; Kito, Y. The opening process of thermal plasma contacts in a post-arc channel after current zero in a flat-type SF6 gas-blast quenching chamber. *J. Phys. D: Appl. Phys.* **1997**, *30*, 407–16.
7. Hartinger, K.T.; Pierre, L.; Cahen, C. Combination of emission spectroscopy and fast imagery to characterize high-voltage SF6 circuit breakers. *J. Phys. D: Appl. Phys.* **1998**, *31*, 2566–76.
8. Kozakov, R.; Kettlitz, M.; Weltmann, K.D.; Steffens, A.; Franck, C.M. Temperature profiles of an ablation controlled arc in PTFE: I. Spectroscopic measurements. *J. Phys. D: Appl. Phys.* **2007**, *40*, 2499–2506.
9. Methling, R.; Khakpour, A.; Götte, N.; Uhrlandt, D. Ablation-Dominated Arcs in CO_2 atmosphere - Part I: Temperature Determination near Current Zero.
10. Paul, K.C.; Sakutay, T.; Takashimay, T.; Ishikawa, M. The dynamic behaviour of wall-stabilized SF_6 arcs contaminated by Cu and PTFE vapours. *J. Phys. D: Appl. Phys.* **1997**, *30*, 103–112.
11. Khalid, R.; Yaqub, K.; Yaseen, S.; Javeed, S.; Ashraf, A.; Janjua, S.A.; Ahmad, S. Sputtering of graphite in pulsed and continuous arc and spark discharges. *Nucl. Instr. and Meth. in Phys. Res. B* **2007**, *263*, 497—502.
12. Bystrzejewski, M.; Łabędź, O.; Lange, H. Diagnostics of carbon arc plasma under formation of carbon-encapsulated iron nanoparticles by optical emission and absorption spectroscopy. *J. Phys. D: Appl. Phys.* **2013**, *46*, 355501.
13. Vekselman, V.; Feurer, M.; Huang, T.; Stratton, B.; Raitses, Y. Complex structure of the carbon arc discharge for synthesis of nanotubes. *Plasma Sources Sci. Technol.* **2017**, *26*, 065019.
14. Becerra, M.; Friberg, A. Arc jets blown by outgassing polymers in air. Proc. XIXth Int. Conf. on Gas Discharges and Their Applications, 2014, Vol. 1, pp. 1–4.
15. Harilal, S.S.; Issac, R.C.; Bindhu, C.V.; Nampoori, V.P.N.; Vallabhan, C.P.G. Optical emission studies of C2 species in laser–produced plasma from carbon. *J. Phys. D: Appl. Phys.* **1997**, *30*, 1703–1709.
16. Park, H.S.; Nam, S.H.; Park, S.M. Optical emission studies of a plume produced by laser ablation of a graphite target in a nitrogen atmosphere. *Bull. Korean Chem. Soc.* **2004**, *25*, 620–626.
17. Camacho, J.J.; Diaz, L.; Santos, M.; Reyman, D.; Poyato, J.M.L. Optical emission spectroscopic study of plasma plumes generated by IR CO2 pulsed laser on carbon targets. *J. Phys. D: Appl. Phys.* **2008**, *41*, 105201.

18. Parigger, C.G.; Hornkohl, J.O.; Nemes, L. Time-resolved spectroscopy diagnostic of laser-induced optical breakdown. *Int. J. Spectroscopy* **2010**, *2010*, 593820.
19. Witte, M.J. Diatomic Carbon Measurements with Laser-Induced Breakdown Spectroscopy. Masters theses, University of Tennessee, 2015.
20. Reynaud, O.; Picard, J.P.; Parizet, M.J. Rotational Temperatures Determined from C_2 Molecular Band Spectra in a Thermal Argon Plasma Interacting with Insulating Materials. *Spectroscopy Letters* **1995**, *28*, 1007–1014.
21. Sakuyama, T.; Amitani, K.; Tanaka, Y.; Uesugi, Y.; Kaneko, S.; Okabe, S. Investigation on Spatial Temperature Decay of Thermal Plasma with Polymer Ablation. *J. Plasma Fusion Res. SERIES* **2008**, *8*, 732–735.
22. Hong, D. Sandolache, G.; Lan, K.; Bauchire, J.M.; Le Menn, E.; Fleurier, C. A radiation source developed for broad band optical absorption spectroscopy measurements. *Plasma Sources Sci. Technol.* **2003**, *12*, 1–7.
23. Günther, K.; Radtke, R. A proposed radiation standard for the visible and UV region. *J. Phys. E: Sci. Inst.* **1975**, *8*, 371–376.
24. Cheon, J.; Kang, H.K.; Zink, J.I. Spectroscopic identification of gas phase photofragments from coordination compound chemical vapor deposition precursors. *Coordination Chem. Rev.* **2000**, *200–202*, 1009–1032.
25. Pearse, R.W.B.; Gaydon, A.G. *The identification of molecular spectra*, 3rd edition ed.; The Whitefriars Press, Ltd., 1963.
26. SpecLine - Spectral line idenfication for atoms and molecules. [Online]. Available: https://www.plasus.de [retrieved December 2019], Smithsonian Astrophyical Observatory, 2018.